Fluctuations of conserved charges with finite size PNJL model

Paramita Deb*

Department of Physics, Indian Institute of Technology Bombay, Powai, Mumbai- 400076, India

Raghava Varma†

Department of Physics, Indian Institute of Technology Bombay Powai, Mumbai-400076, India

(Dated: February 27, 2024)

Baryon, charge and strangeness fluctuations have been investigated in finite size Polyakov loop enhanced Nambu–Jona-Lasinio model. Multiple reflection expansion method has been incorporated to include the surface and curvature energy along with the system volume. The results of different fluctuations are then compared with the available experimental data from the heavy ion collision. Results show both qualitative and quantitative similarities with the experimental data after using the subensemble acceptance method. Phase diagram for the infinite and finite size PNJL model has been studied to estimate the critical end point.

PACS numbers: 12.38.AW, 12.38.Mh, 12.39.-x

I. INTRODUCTION

The earliest universe, moments after the big bang, consisted of a quark-gluon-plasma state. Subsequently, a phase transformation to hadronic phase occured. It is with this goal of recreating the primodial universe that the heavy ion collision experiments at Relativistic Heavy Ion Collider (RHIC) at BNL and Super Proton Synchrotron (SPS) at CERN are conducted. The primary objectives of both these experiments are to study the strongly interacting matter at finite temperature and density and to map the QCD phase diagram and estimate the critical end point (CEP). The phase diagram itself conveys the various interplay of strongly interacting matter and is necessary to understand the effects at finite temperature and density, not unlike to the phase transformation that has occured in the early universe. However, unlike early universe, the fireball created in the experiments have a finite size and volume. In the heavy ion collision experiments, after the formation of quark gluon plasma phase (QGP), matter expands and different chemical and kinetic interactions cease (called the freeze out point) leading to the hadronic phase. Meanwhile, the first order phase transition from quark gluon plasma (QGP) phase to the hadronic phase becomes continuous which indicates the crossover transition [1, 2]. While, a second order phase transformation occurs at CEP.

The detection of particles before the cessation of all the inelastic and elastic collisions at the freeze out condition can point to the location of the freeze out point which in turn

* paramita.deb83@gmail.com

† varma@phy.iitb.ac.in

can locate the critical point. Necessarily, experiments are being conducted to bring the freeze out point close to the critical point by varying the collision center of mass energy $\sqrt{s}$ [3] of the colliding nuclei. However, nature of the experimental observables change near the critical point. Hence, in order to conduct experiment near the critical region, suitable experimental observables such as conserved quantities are needed. Specifically, the fluctuations of these conserved quantities show non-monotonous behavior near the critical region. Generally, the fluctuations of experimental observables are defined as the variance and higher non-Gaussian moments of the event-by-event distribution of the observable at each event in ensemble of many events. Further more, the magnitude of these fluctuations of the conserved quantities such as net-baryon (ΔB), net-strangeness (ΔS) and net-charge (ΔQ) as well as the correlation length (ξ) diverge at the critical point. Therefore, the non-monotonic behaviour of these fluctuations of the higher order moments of these conserved quantities could be the signature of the critical point [4, 5]. The QCD inspired models [6–33] further indicate that the net conserved quantum numbers (B, Q and S) are related to the conserved number susceptibilities ($\chi_x = \langle(\delta N_x)^2\rangle/VT$ where x can be either B, S or Q and V is the volume), which generally agree with the lattice QCD models [34–47]. Further, the distributions of the conserved quantum numbers are non-Gaussian and the susceptibilities diverge near the critical region. It may be remarked that susceptibilities are also related to the higher non-Gaussian moments of these conserved quantities such as skewness, S ($\sim \xi^{4.5}$), and kurtosis, ($\sim \xi^{7.0}$). Further, higher order susceptibilities are much more sensitive to the correlation length which can be very useful in the search of CEP. As these higher order moment ratios of the conserved quantities ($s\sigma = (\chi_x^3/\chi_x^2)$ and $\kappa\sigma^2 = \chi_x^4/\chi_x^2$) are volume independent, it can be constructed to cancel out the system size dependency in line with the experimental results. Susceptibilities of different conserved charges have been also computed with respect to the quark chemical potential (μ) in the Polyakov loop coupled quark-meson (PQM) model [26–30], its improved versions [48–51], and PNJL model [15, 19, 52] with finite volume effects.

In contrast to the experiments, most of the earlier QCD inspired theoretical approaches do not consider the finite volume effect such as the Nambu–Jona-Lasinio (NJL) model [53] and it's extension the Polyakov loop Nambu–Jona-Lasinio (PNJL) model [6–8, 10–33]. Nonetheless, recent theoretical models incorporate the effects of finite volume and have been addressed by many models such as non-interacting bag model [54], chiral perturbation theory [55, 56], both the NJL model and the PNJL model with finite volume effects [57, 58], linear sigma model [59, 60] and also by the first principle study of pure gluon theory on space time lattices [61, 62]. Specifically, in the Polyakov loop Nambu–Jona-Lasinio (PNJL) model it has been concluded that as the volume decreases, the critical temperature for the crossover transition decreases. Additionally, for lower volumes, CEP shifts to a region having both lower chemical potential (μ) and lower temperature (T) [19, 52]. Although, broadly both the Lattice calculations and QCD-based models indicate that the fluctuation of strongly interacting matter at zero density show significant volume dependence which might be relevant to study the formation of fireball in heavy-ion collisions; the model was simplistic. It did not consider the sizes explicitely and the finite volume contribution was incorporated as a boundary condition in the lower limit of the integral of thermodynamic potential $p_{min} = \pi/R = \lambda$, where R is the lateral size of the finite volume system [19]. Further, the surface and curvature effects were neglected, the infinte sum had been considered as an integration over a continuous variation of momentum albeit with the lower cut-off, and modifications to the mean-field parameters due to finite size effects have not been considered. A way to improve the surface and curvature effects that bound the finite volume of PNJL system would be through the multiple reflection expansion (MRE) method [57, 63–65] compared to previous finite volume calculations, MRE describes a sphere with proper boundary conditions rather than a cube, which is more natural to study the problem of QGP fireball in heavy ion collision. In order to compare the theoretical results with the experimental data, it is important to obtain the observables within the similar ensembles. The conserved quantities obtained in the theoretical approaches are calculated in the grand canonical ensemble. Whereas the conserved quantities are measured in a subvolume system in the heavy ion collision experiments opposed to the case of the grand canonical ensemble where the system can freely exchange the charge with an external heat bath. In order to resolve the discrepancy the subensemble acceptance method has been proposed to measure the fluctuations of the conserved quantities in the experimental measurements [66].

In the light of above discussions, the current work will emphasis on the 3 flavor finite size finite density PNJL model with MRE formalism as well as infinite volume PNJL model to study the susceptibilities of different conserved charges and compare them to both the recent experimental findings. The presentation of the work follows as a thermodynamic description of the three flavor finite size PNJL model with MRE formalism, calculation of the fluctuations and variation of skewness, kurtosis of conserved charges, higher moments with collision energies, and possible location of the critical end point.

II. THE PNJL MODEL

The PNJL model consists of both four quark and six quark interaction terms and a Polyakov loop which represents the gluonic degrees of freedom. The model nicely captures the confinement and chiral symmetry restoration properties of strongly interacting matter. We shall consider the 2+1 flavor PNJL model with six quark interactions.

The gluon dynamics is described by the chiral point couplings between quarks (present in the NJL part) and a background gauge field representing the Polyakov Loop dynamics. The Polyakov line is represented as,

$$L(\bar{x}) = \mathcal{P}\exp[i\int_0^\beta d\tau A_4(\bar{x},\tau)] \tag{1}$$

where $A_4 = iA_0$ is the temporal component of Eucledian gauge field $(\bar{A}, A_4)$, $\beta = \frac{1}{T}$, and $\mathcal{P}$ denotes path ordering. $L(\bar{x})$ transforms as a field with charge one under global Z(3) symmetry. The Polyakov loop is then given by $\Phi = (Tr_c L)/N_c$, and its conjugate by, $\bar{\Phi} = (Tr_c L^\dagger)/N_c$. Consequently, the Polyakov loop potential can be expressed as,

$$\frac{\mathcal{U}'(\Phi[A],\bar{\Phi}[A],T)}{T^4} = \frac{\mathcal{U}(\Phi[A],\bar{\Phi}[A],T)}{T^4} - \kappa\ln(J[\Phi,\bar{\Phi}]) \tag{2}$$

where $\mathcal{U}(\phi)$ is a Landau-Ginzburg type potential commensurate with the Z(3) global symmetry. Here we choose a form given in [7],

$$\frac{\mathcal{U}(\Phi,\bar{\Phi},T)}{T^4} = -\frac{b_2(T)}{2}\bar{\Phi}\Phi - \frac{b_3}{6}(\Phi^3+\bar{\Phi}^3) + \frac{b_4}{4}(\bar{\Phi}\Phi)^2, \tag{3}$$

where

$$b_2(T) = a_0 + a_1 exp(-a2\frac{T}{T_0})\frac{T_0}{T} \tag{4}$$

b_3 and b_4 being constants. The second term in eqn.(2) is the Vandermonde term which replicates the effect of SU(3) Haar measure and is given by,

$$J[\Phi, \bar{\Phi}] = (27/24\pi^2)\left[1 - 6\Phi\bar{\Phi} + 4(\Phi^3 + \bar{\Phi}^3) - 3(\Phi\bar{\Phi})^2\right]$$

The parameters of the polyakov loop potential are typically determined by fitting a few thermodynamic quantities such as pressure as a function of temperature which have been obtained a-priori from Lattice QCD computations. The set of values chosen have been reproduced below in table I [15].

Interaction	$T_0(MeV)$	a_0	a_1	a_2	b_3	b_4	κ
6-quark	175	6.75	-9.0	0.25	0.805	7.555	0.1

TABLE I. Parameters for the Polyakov loop potential of the model.

Meanwhile, for the quarks, we shall use the usual form of the NJL model except for the substitution of a covariant derivative containing a background temporal gauge field. Thus the 2+1 flavor Lagrangian may be written as,

$$\begin{aligned}\mathcal{L} = \sum_{f=u,d,s} \bar{\psi}_f \gamma_\mu i D^\mu \psi_f - \sum_f m_f \bar{\psi}_f \psi_f + \sum_f \mu_f \gamma_0 \bar{\psi}_f \psi_f + \frac{g_S}{2} \sum_{a=0,\ldots,8} [(\bar{\psi}\lambda^a\psi)^2 + (\bar{\psi} i\gamma_5 \lambda^a \psi)^2] \\ - g_D[det\bar{\psi}_f P_L \psi_{f'} + det\bar{\psi}_f P_R \psi_{f'}] \\ - \mathcal{U}'(\Phi[A], \bar{\Phi}[A], T)\end{aligned}$$

where f denotes the flavors u, d or s, respectively. The matrices $P_{L,R} = (1 \pm \gamma_5)/2$ are the left-handed and right-handed chiral projectors, and the other terms have their usual meaning, described in details in Refs. [13–19]. This is analogous to the BCS theory of superconductor, where the pairing of two electrons leads to a condensation. Similarly, in the chiral limit the NJL model exhibits dynamical breaking of the $SU(N_f)_L \times SU(N_f)_R$ symmetry to $SU(N_f)_V$ symmetry (N_f being the number of flavors). As a result the operators ψ and $\bar{\psi}$ pair and generate nonzero vacuum expectation values. The quark condensate is given as,

$$\langle \bar{\psi}_f \psi_f \rangle = -iN_c \mathcal{L}t_{y\to x^+}(trS_f(x-y)), \tag{5}$$

where the trace is over color and spin states. The self-consistent gap equation for the constituent quark masses are,

$$M_f = m_f - g_S\sigma_f + g_D\sigma_{f+1}\sigma_{f+2} \tag{6}$$

where $\sigma_f = \langle\bar{\psi}_f\psi_f\rangle$ denotes chiral condensate of the quark with flavor f. Here if we consider $\sigma_f = \sigma_u$, then $\sigma_{f+1} = \sigma_d$ and $\sigma_{f+2} = \sigma_s$, the expression for σ_f at zero temperature ($T = 0$) and chemical potential ($\mu_f = 0$) may be written as [15],

$$\sigma_f = -\frac{3M_f}{\pi^2}\int^{\Lambda}\frac{p^2}{\sqrt{p^2+{M_f}^2}}dp, \tag{7}$$

Λ being the three-momentum cut-off. This cut-off have been used to regulate the model because it contains couplings with finite dimensions which makes the model non-renormalizable. The parameter values for the quark interaction part Λ, g_S and g_D can be obtained by fitting the physical observables like pion mass, kaon mass, pion decay constant obtained from the experimental observation. These have been listed in table II. Here we consider the Φ, $\bar{\Phi}$ and σ_f fields in the mean field approximation (MFA).

Model	$m_u(MeV)$	$m_s(MeV)$	$\Lambda(MeV)$	$g_S\Lambda^2$	$g_D\Lambda^5$
With 6-quark	5.5	134.76	631	3.67	9.33

TABLE II. Parameters of the Fermionic part of the model.

It may be remarked that the model formulation described above does not consider the finite volume effects. The finite volume effect will be incorporated in the study by multiple reflection expansion method (MRE) by considering the system as a spherical droplet. The interaction between different quarks can be determined by the reflection of the quarks multiple times from the boundary of the spherical droplet. The effect of the interactions can be determined by applying proper boundary conditions. The MRE formalism is described in the following section.

III. MULTIPLE REFLECTION EXPANSION

Multiple reflection expansion technique was first formulated by [63] to determine the distribution of eigenvalues of the equation $\triangle\phi + E\phi = 0$ for a finite volume V but for sufficiently smooth surface with boundary condition $\partial\phi/\partial n = \kappa\phi$. This technique has been further applied to various problems in nuclear physics including the density of states for massive quarks in a bag [64]. In an ideal Fermi-gas, the energy of a system composed of quark flavors is given by

$$E = \sum_i(\Omega_i + N_i\mu_i) + BV \tag{8}$$

Here Ω_i, N_i and μ_i denote thermodynamic potentials, total number of quarks and chemical potentials respectively. B is a constant associated with the volume. Generally, in the multiple reflection expansion framework, the thermodynamical quantities can be derived from the density of states in the form shown below 9.

$$\frac{dN_i}{dp} = 6[\frac{p^2V}{2\pi^2} + f_S(\frac{m_i}{p})kS + f_C(\frac{m_i}{p})C + \ldots] = \frac{p^2\rho_{MRE}}{2\pi^2} \tag{9}$$

where area $S = \oint dS = 4\pi R^2$ and curvature $C = 8\pi R$ for a sphere. The density of states for the quarks in the fireball can be written as

$$\rho_{i,MRE}(p, m_i, R) = 1 + \frac{6\pi^2}{pR} f_{i,S} + \frac{12\pi^2}{(pR)^2} f_{i,C} \tag{10}$$

where the surface contribution to the density of states is

$$f_{i,S} = -\frac{1}{8\pi}(1 - \frac{2}{\pi} arctan \frac{p}{m_i}) \tag{11}$$

and the curvature contribution is given by Madsen's ansatz [64]

$$f_{i,C} = \frac{1}{12\pi^2}[1 - \frac{3p}{2m_i}(\frac{\pi}{2} - arctan \frac{p}{m_i})] \tag{12}$$

However, for a range of small momenta, the density of states becomes negative. These non-physical negative values are removed by introducing an infrared (IR) cutoff in momentum space [57]. The IR cut-off $\lambda_{i,IR}$ is the largest solution of the equation $\rho_{i,MRE}(p, m_i, R) = 0$ with respect to the momentum p. Further, in order to obtain the thermodynamic quantities, following replacements are necessary

$$\int_0^\infty \cdots \frac{d^3p}{(2\pi)^3} \rightarrow \int_{\lambda_{i,IR}}^\infty \cdots \rho_{i,MRE} \frac{d^3p}{(2\pi)^3} \tag{13}$$

Although, in finite system PNJL model, an introduction of a system size (R) dependent lower momentum cutoff λ can account for the finite volume effects [19], the contribution of the surface and curvature effects remain unclear. In this scenario, a mass dependent lower momentum cutoff λ_{IR} is introduced and the mathematical formulation is described in the following section. Briefly, the value of λ_{IR} for different values of R and u, d and s masses have been calculated. For $R = 2fm$, the lower cut-off for different masses are $\lambda_{u,IR} = 75.2fm^{-1}$ and $\lambda_{s,IR} = 131.0fm^{-1}$ and for $R = 4fm$, the lower cut-offs are $\lambda_{u,IR} = 40.0fm^{-1}$ and $\lambda_{s,IR} = 75.1fm^{-1}$. u and d quarks have same value for λ_{IR}.

IV. THERMODYNAMIC POTENTIAL

The thermodynamic potential for the multi-fermion interaction in the mean field approximation (MFA) of the PNJL model with MRE contribution can be written as,

$$\begin{aligned}
\Omega = \mathcal{U}'[\Phi, \bar{\Phi}, T] + 2g_S \sum_{f=u,d,s} {\sigma_f}^2 - \frac{g_D}{2}\sigma_u\sigma_d\sigma_s - 6\sum_f \int_0^\Lambda \frac{d^3p}{(2\pi)^3} \rho_{i,MRE} E_{pf} \Theta(\Lambda - |\boldsymbol{p}|) \\
- 2\sum_f T \int_0^\infty \frac{d^3p}{(2\pi)^3} \rho_{i,MRE} [\ln \left\{ 1 + 3\left(\Phi + \bar{\Phi} e^{-\frac{(E_{pf}+\mu)}{T}}\right) e^{-\frac{(E_{pf}+\mu)}{T}} + e^{-3\frac{(E_{pf}+\mu)}{T}66} \right\} \\
+ \ln \left\{ 1 + 3\left(\bar{\Phi} + \Phi e^{-\frac{(E_{pf}+\mu)}{T}}\right) e^{-\frac{(E_{pf}+\mu)}{T}} + e^{-3\frac{(E_{pf}+\mu)}{T}} \right\}] \qquad (14) \\
= \mathcal{U}' + \Omega_{cond} + \Omega_{vac} + \Omega_{med} \qquad (15)
\end{aligned}$$

where $E_{pf} = \sqrt{p^2 + M_f^2}$ is the single quasi-particle energy, $\sigma_f^2 = (\sigma_u^2 + \sigma_d^2 + \sigma_s^2)$ and $\sigma_f^4 = (\sigma_u^4 + \sigma_d^4 + \sigma_s^4)$. Here $\mathcal{U}'$ is the Polyakov loop potential, Ω_{cond} consists of second and third interaction term, Ω_{vac} is the vaccum term and Ω_{med} is the medium dependent term. In the above integrals, the vacuum integral has a cutoff Λ whereas the medium dependent integrals have been extended to infinity.

In the present study we have two sets of parameter (a) PNJL-6-quark for $R = 2fm$, (b) PNJL-6-quark for $R = 4fm$. In the figure 1, the temperature dependance of constituent

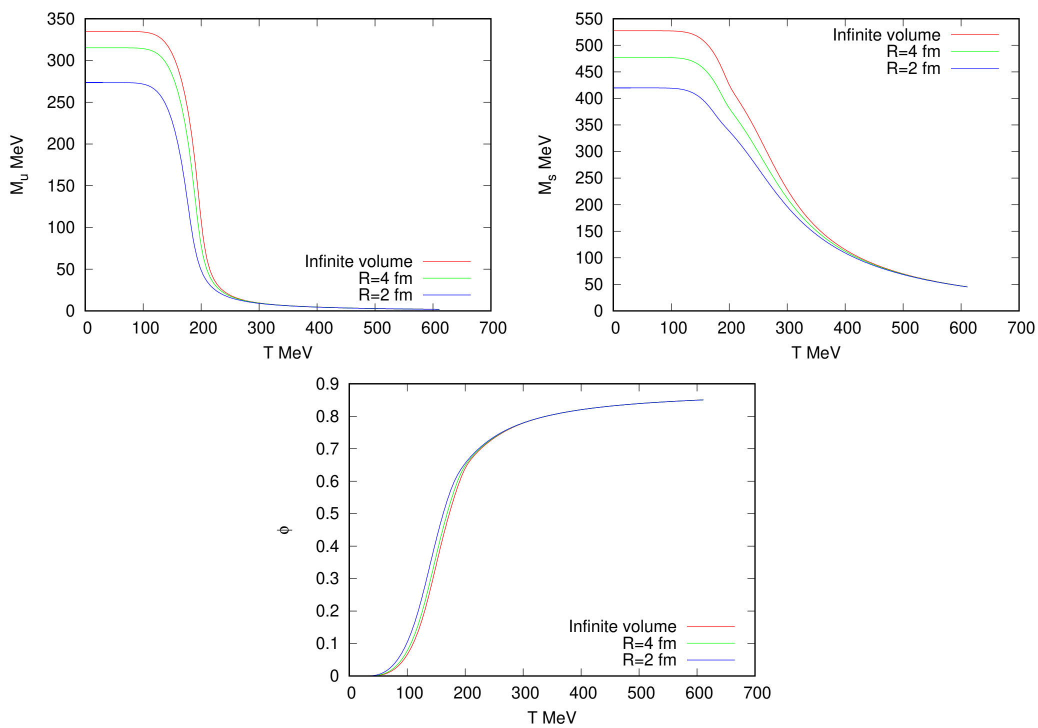

FIG. 1. (Color online) Constituent mass of u quark M_u and constituent mass of s quark M_s have been plotted as a function of temperature T at $\mu = 0$ for finite and infinite volume system. Polyakov loop ϕ_u has been plotted as a function of T at $\mu = 0$ for finite and infinite volume. PNJL model with infinite volume has been denoted by red color, PNJL model with $R = 4fm$ has been denoted by green color and PNJL model with $R = 2fm$ has been denoted by blue color.

mass of u and s quark and Polyakov loop ϕ have been plotted. While the mass M_u is greater in the infinite volume system than the finite volume system in the low temperature region, at higher temperature they attain simillarity. For infinite volume the mass of u quark is around $334MeV$ and it drops down to $274MeV$ for finite volume system with $R = 2fm$. At high temperatures, all the masses tends toward zero. The trends remain similar for s quark also. In contrast to the quarks, the Polyakov loop ϕ shows weak volume dependence. The critical temperature at $\mu = 0$ for infinite volume system is $T_c = 172.0MeV$, for finite volume system with $R = 4fm$ is $T_c = 167.0MeV$, and for $R = 2fm$ it is $T_c = 158.0MeV$.

A. Taylor expansion of pressure

The freeze-out curve $T(\mu_B)$ in the $T-\mu_B$ plane and the dependence of the baryon chemical potential on the center of mass energy in nucleus-nucleus collisions can be parametrized as demonstrated by Cleymans et al. [67]

$$T(\mu_B) = a - b\mu_B^2 - c\mu_B^4 \tag{16}$$

where $a = (0.166 \pm 0.002)\ GeV$, $b = (0.139 \pm 0.016)\ GeV^{-1}$, $c = (0.053 \pm 0.021)\ GeV^{-3}$ and

$$\mu_B(\sqrt{s}_{NN}) = d/(1 + e\sqrt{s}_{NN}) \tag{17}$$

with d, e as given by Karsch et al. [68].

The ratio of baryon (μ_B) to strangeness chemical potential (μ_S) on the freeze-out curve shows a weak dependence on the collision energy

$$\frac{\mu_S}{\mu_B} \sim 0.164 + 0.018\sqrt{s}_{NN} \tag{18}$$

Although, several methods for new parametrization of the freeze-out curve in the T vs μ_B plane have been proposed (e.g. Borsanyi et al. [69]), the old method where the values of baryon, charge and strangeness chemical potentials are available with respect to freeze out temperature and BES energy has been used [68], so as not to be restricted to the T - μ_B plane alone. The old method ensures evaluation of all the values of the chemical potential.

The pressure of the strongly interacting matter can be written as,

$$P(T, \mu_B, \mu_Q, \mu_S) = -\Omega(T, \mu_B, \mu_Q, \mu_S), \tag{19}$$

where T is the temperature, μ_B is the baryon (B) chemical potential, μ_Q is the charge (Q) chemical potential and μ_S is the strangeness (S) chemical potential. From the usual thermodynamic relations the first derivative of pressure with respect to quark chemical potential μ_q is the quark number density and the second derivative corresponds to the quark number susceptibility (QNS).

Minimizing the thermodynamic potential numerically with respect to the fields σ_u, σ_d, σ_s, Φ and $\bar{\Phi}$, the mean field value for pressure can be obtained using the equation (19) [15]. The scaled pressure obtained in a given range of chemical potential at a particular temperature can be expressed in a Taylor series as,

$$\frac{p(T, \mu_B, \mu_Q, \mu_S)}{T^4} = \sum_{n=i+j+k} c_{i,j,k}^{B,Q,S}(T)\left(\frac{\mu_B}{T}\right)^i\left(\frac{\mu_Q}{T}\right)^j\left(\frac{\mu_S}{T}\right)^k \tag{20}$$

where,

$$c_{i,j,k}^{B,Q,S}(T) = \frac{1}{i!j!k!}\frac{\partial^i}{\partial(\frac{\mu_B}{T})^i}\frac{\partial^j}{\partial(\frac{\mu_Q}{T})^j}\frac{\partial^k(P/T^4)}{\partial(\frac{\mu_S}{T})^k}\Big|_{\Delta\mu_{B,Q,S}} \tag{21}$$

where $\Delta\mu = (\mu_X - \mu_0)$ and $\mu_X = \mu_B$ or μ_Q or μ_S. μ_X are the freeze out chemical potentials and are related to the flavor chemical potentials μ_u, μ_d, μ_s as,

$$\mu_u = \frac{1}{3}\mu_B + \frac{2}{3}\mu_Q, \quad \mu_d = \frac{1}{3}\mu_B - \frac{1}{3}\mu_Q, \quad \mu_s = \frac{1}{3}\mu_B - \frac{1}{3}\mu_Q - \mu_S \tag{22}$$

To extract the Taylor coefficients, first the pressure is obtained as a function of chemical potentials for each value of freeze out temperature and then fitted to a polynomial about $\Delta\mu$ using the gnu-plot fit program [70]. Further, instead of differentiating the pressure with respect to μ sucessivively to obtain the thermodynamic potential Ω (requiring higher order derivatives, upto 4^{th} order), the Taylor expansion around $\Delta\mu$ has been preferred in this study. This ensures both an easy determination and comparision of the coefficients. Stability of the fit has been checked by varying the ranges of fit and simultaneously keeping the values of least squares to 10^{-10} or even less.

B. Subensemble acceptance method

In the theoretical calculations, the conserved charges have been measured considering the system as a grand canonical ensemble (GCE). However, in the experimental measurements, the total net conserved charges can not fluctuate as opposed to the GCE where the system can freely exchange the charge with an external heat bath. In order to connect the measurements of the experimental cumulants of conserved charge fluctuations to the grand canonical susceptibilities, subensemble acceptance method has been used [66]. The spatially uniform thermal system with volume V, temperature T and conserved charges $X = B$, Q or S has been described by the canonical partition function $Z(T, V, X)$ with a subsystem of fixed volume $V_1 = \alpha V$ within the whole system. V_1 can freely exchange the conserved charges with rest of the system. The cumulants, skewness and kurtosis are calculated as follows

$$\frac{K_3[X_1]}{K_2[X_1]} = (1-2\alpha)\frac{\chi_3^X}{\chi_2^X} \tag{23}$$

$$\frac{K_4[X_1]}{K_2[X_1]} = (1-3\alpha\beta)\frac{\chi_4^X}{\chi_2^X} - 3\alpha\beta(\frac{\chi_3^X}{\chi_2^X})^2 \tag{24}$$

where $X = B, QorS$ and $K[X_1]$ are the cumulants of the distribution of conserved charges $X_1 = B_1$, Q_1 or S_1 within the subsystem. α can vary from 0 to 1 and $\beta = (1-\alpha)$ where α is the probability of the independent acceptance of particles in a subvolume system from the entire volume. If α is known, the equations can be used to express the grand canonical ensemble, cumulants ratios in terms of those of the subsystem and vice-versa. In this work the subensemble acceptance method has been applied to the cumulants measured in the experiment to compare them with the theoretical model data.

C. Results

The experimental results for volume independent cumulant ratios of net-proton, net-kaon and net-charge number distribution have been obtained for all BES energies $\sqrt{s}_{NN} = 7.7, 11.5, 14.5, 19.6, 27, 39, 62.4$ and $200GeV$ for top central and peripheral collisions [71–73]. We have presented our results for finite size PNJL model including the MRE formalism for six-quark interactions and compared them against the experimental data. Nonetheless, for a meaningful comparison of moments calculated theoretically with the experimental data, a degree of confidence in the measured system volumes is necessary. However, measurement of the system size in the experiments is not trivial. Recent study of the LHC energy shows that the system size of strongly interacting matter is in the range of $1.6-4.5fm$ [74]. Typically, ratios of moments are considered to eliminate the volume factor, a valid assumption if the interactions are small and the volume factor scales out. Though, in the purely hadronic or partonic phases, one may observe such a scaling of the moments with system size, it may not hold near the critical region. There, large scale fluctuations are dominant and the system deviates from a stable thermodynamic phase.

The correlation length and the magnitude of fluctuations are important quantity as they diverge at the critical end point. Because of the finite size effects, the correlation length takes a finite volume in the range $\sim 2-3fm$. Higher non-Gaussian moments such as skewness and kurtosis are much more sensitive in the critical region rendering them important observables for locating the CEP. In this Figure (2), we have plotted $S\sigma$ (which is the ratio of the third order to second order moment) and $k\sigma^2$ (ratio of fourth order to second order moment) of the baryon fluctuation with respect to collision energy for the PNJL model with infinite volume and also for the finite size with $R = 2fm$ and $R = 4fm$. Here S and k represent the skewness and the kurtosis of higher order fluctuations, respectively.

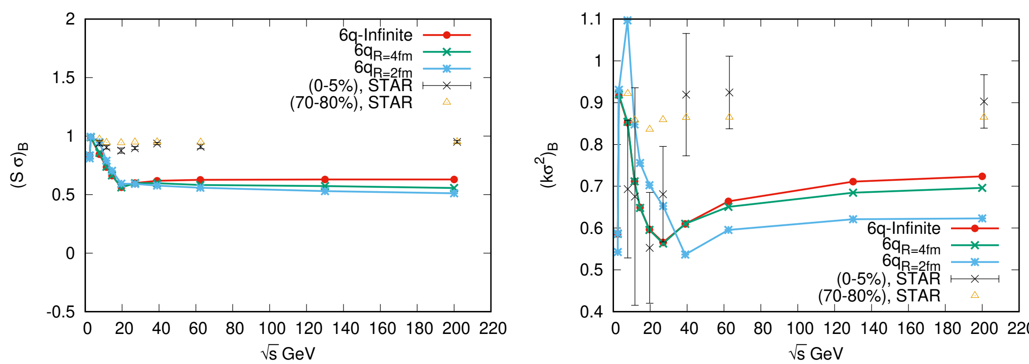

FIG. 2. (Color online) $S\sigma$ (top panel) and $k\sigma^2$ (bottom panel) of baryon fluctuation have been plotted with respect to collision centrality. PNJL model with infinite volume has been denoted by red color, PNJL model with $R = 4fm$ has been denoted by green color and PNJL model with $R = 2fm$ has been denoted by blue color. The model data has been compared with the recent experimental data available from STAR. Central collision with $(0\% - 5\%)$ centrality has been denoted by black color with error bar. Peripheral collision with $(70\% - 80\%)$ centrality has been denoted with yellow color.

Interestingly, the plot of the $S\sigma$ with collision energy (Figure 2) shows higher value of fluctuation around $\sqrt{s} = 11.5GeV$. After $\sqrt{s} = 11.5GeV$ the fluctuations decrease sharply; more so for the model data compared to the experimental data. Beyond $\sqrt{s} = 20GeV$ the fluctuation becomes constant similar to the experimental value. Necessarily, the nature of fluctuation may indicate that the critical region lies below $\sqrt{s} = 20GeV$. Similar nature has been also observed for the net-proton fluctuation in experiment. A comparison of the model (PNJL with MRE) data with the experimental data for $(0\%-5\%)$ centrality and $(70\%-80\%)$ centrality is also presented. Though, there is a qualitative match, the values disageee. It may be remarked that the available experimental data is for net-proton fluctuations while the baryon fluctuation are calculated here. Meanwhile, the $k\sigma^2$ shows a sharp rise in fluctuation around $\sqrt{s} = 11.5GeV$ and a minimum around $20-40GeV$ for collision centrality.

Interestingly, the initial values match quite well with the experimental value though for large collision energies (after $\sqrt{s} = 40GeV$) they differ. Nonetheless, both the ratios of baryon fluctuations are in good agreement with the experimental result qualitatively. [71].

Figure 3 shows the $S\sigma$ and $k\sigma^2$ for charge fluctuation with respect to the collision centrality. As evident from the plot, $S\sigma$ attains a maxima around collision energy of $20 - 40GeV$. The value of fluctuation for infinite volume is significantly large for $R = 2fm$ than for $R = 4fm$. The trend is in consonance with the experiments where the value of $S\sigma$ is almost zero around $\sqrt{s} = 200GeV$ and increases with the decrease in collision energies. Nonetheless, the values do not exactly match with the experimental data. Meanwhile, $k\sigma^2$ of charge fluctuation with respect to collision centrality shows a minimum around $\sqrt{s} = 20GeV$ for both finite and infinite volume. In contrast, the experimental result shows almost a steady value of $k\sigma^2$ after initial turbulance at lower beam energy [72]. Though, the model data also shows uniform behavior above $\sqrt{s} = 20GeV$, but there is an enhancement of fluctuation in the collision energy range of $7.7 - 20GeV$.

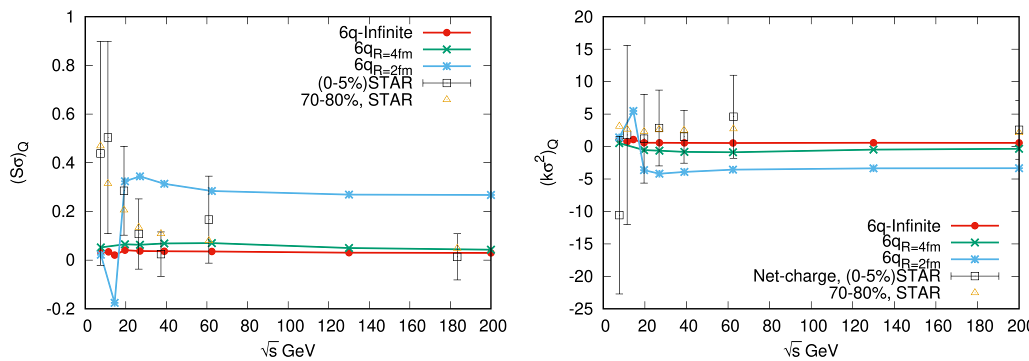

FIG. 3. (Color online) $S\sigma$ (top panel) and $k\sigma^2$ (bottom panel) of charge fluctuation have been plotted with respect to collision centrality.

Figure (4) shows the variation of strangeness fluctuations (C_3/C_{2_S} and C_4/C_{2_S}) with respect to different collision energies for the PNJL model. In recent experimental data no significant deviation of the strangeness fluctuations has been found with respect to the Poisson expectation value within statistical and systematic uncertainties for both the moments [73]. $S\sigma$ for PNJL model with infinite volume and finite volume show similar behavior as the experimental results. However a slight increase in fluctuation below $\sqrt{s} = 20GeV$, $\mu_S = 105MeV$ and $T = 160MeV$ for both finite volume and infinite volume system was observed. The fluctuations are higher for infinite volume system. $k\sigma^2$ also shows similar trend as $S\sigma$. For the collision energy below $\sqrt{s} = 10$ GeV, there is an sharp drop of fluctuation for the PNJL model with MRE. Here also, quantitative variance in the model values and the experimental data were noted.

We hypothesize that the difference between the experimental result and the PNJL model data is due to the difference of statistical ensembles taken for the evaluation. Thus, it is necessary to analyze the experimental data through subensemble acceptance method described in the literatures [66] to relate the cumulants with the grand canonical ensemble. In order to compare the ratios of different order cumulants, the equations described previously (24) has been used. Here three different values of alpha have been considered ($\alpha = 0.05, 0.1, 0, 2$).

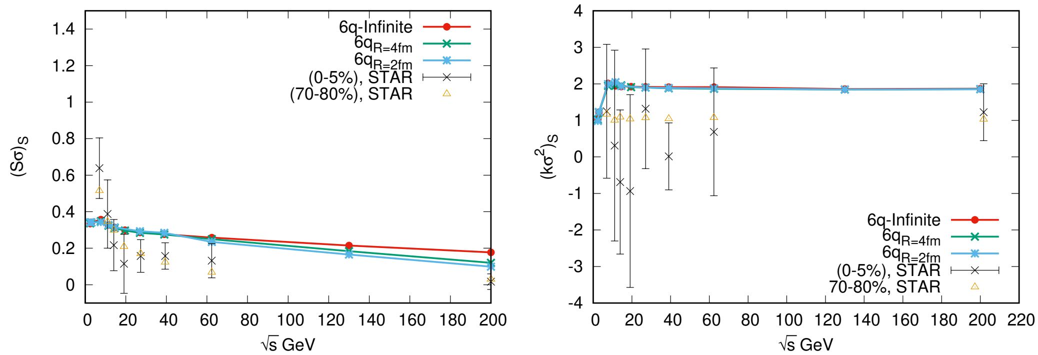

FIG. 4. (Color online) $S\sigma$ (top panel) and $k\sigma^2$ (bottom panel) of strangeness fluctuation have been plotted with respect to collision centrality.

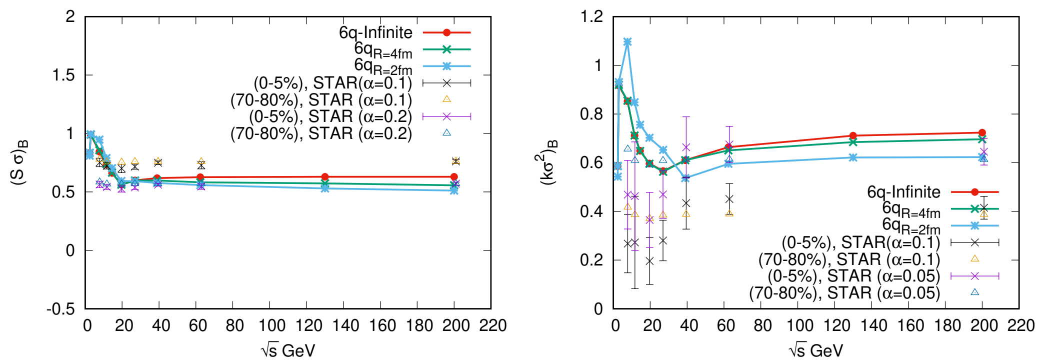

FIG. 5. (Color online) $S\sigma$ (top panel) and $k\sigma^2$ (bottom panel) of baryon fluctuation have been plotted with respect to collision centrality.

The figure 5 represents the $S\sigma$ and $k\sigma^2$ of baryon fluctuations where the experimental data for both $0-5\%$ centrality and $70-80\%$ centrality has been modified by subensemble acceptance method. The data obtained from the MRE modifed PNJL model shows not only qualitative similarity but also quantitatively values are in good agreement with the experimental measurements. For $S\sigma$ the model data fall within the range of experimental values with $\alpha = 0.1$ and $\alpha = 0.2$. Further, for $k\sigma^2$ the model datas are only slightly above the expermental data. It is evident that with fine tuning the value of α, an exact quantitative match between experimental values and theoretical datas can be achieved. In essence, validating the MRE modified PNJL model. The figure 6 represents the $S\sigma$ and $k\sigma^2$ for charge fluctuations. Again, the model data fall in the similar range of experimental values. Meanwhile, for $R = 2fm$, higher value of fluctuations were noted compared to both the infinite volume and finite volume system with $R = 4fm$. Nonethess, a disparity between the experimental data and the MRE modified PNJL data was noted for the strangeness fluctuation. The figure 7 shows the $S\sigma$ and $k\sigma^2$ of strangeness fluctuation. The values seem to be higher than the experimental datas with $\alpha = 0.1, 0.2$.

However the exact match of the model data with the experimental data depends on the fine tuning of the α parameter. The difference between the experimental data and

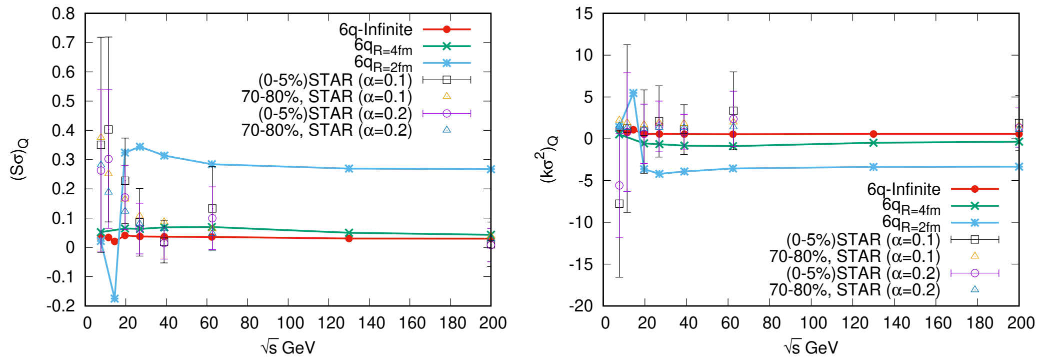

FIG. 6. (Color online) $S\sigma$ (top panel) and $k\sigma^2$ (bottom panel) of charge fluctuation have been plotted with respect to collision centrality.

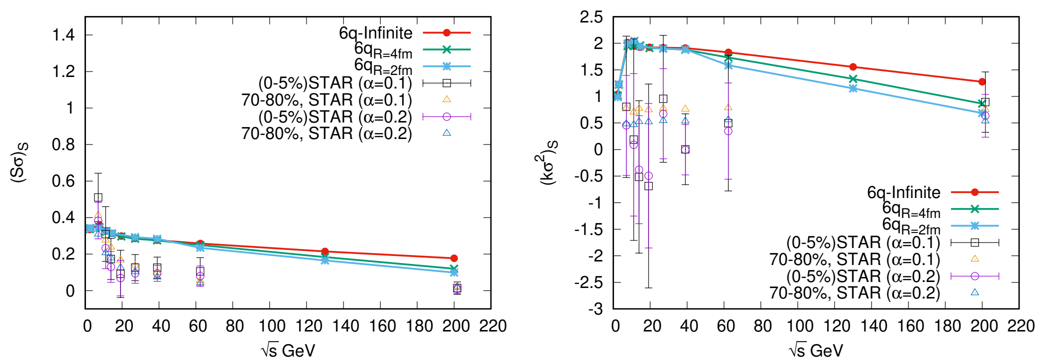

FIG. 7. (Color online) $S\sigma$ (top panel) and $k\sigma^2$ (bottom panel) of strangeness fluctuation have been plotted with respect to collision centrality.

PNJL model data could be because of different statistical ensembles. Hence in order to relate the model data with the experimental data subensemble acceptance method has been utilised to consider the experimental data in a grand canonical ensemble. The quantitative difference between the experimental data and the PNJL model data has been decreased by incorporating the subensemble acceptance method.

D. Phase Diagram

As emphasized earlier, the phase diagram is one of the most interesting phenomenon pertaining to the strongly interacting matter. The phase diagrams are usually obtained by identifying the critical temperature (a discontinuity in the light quark chiral condensate or the maximal point of the derivative with respect to the temperature) for different chemical potentials. In the region where the temperature is less than T_C and the chemical potential is greater than μ_B, the chiral and deconfinement transitions are first order. The critical end point (CEP) separates the crossover transition from the first order phase transition. In the figure (8) the phase diagram for the PNJL model with infinite volume and finite volume with MRE approximation are shown. The position of CEP shifts to the increasingly lower

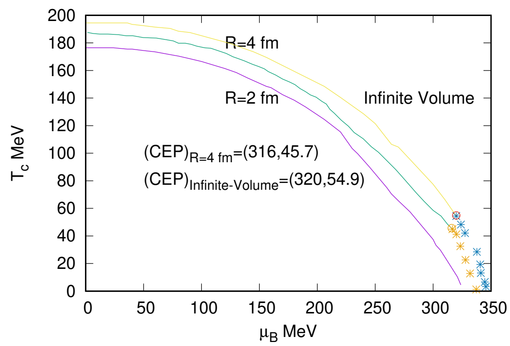

FIG. 8. (Color online)Phase diagram of the PNJL model for infinite and finite volume system with $R = 4fm$ and $R = 2fm$. PNJL model for infinite volume has been denoted by yellow color (crossover part) and blue color (first order), for finite volume system with $R = 4fm$ has been denoted by green color (crossover) and orange color (first order) and the system with $R = 2fm$ has been denoted by magenta color. CEP for infinite volume system is $(\mu_B, T_C = (320, 54.9)MeV)$ and for finite volume system with $R = 4fm$ is $(\mu_B, T_C = (316, 45.7)MeV)$.

temperatures as the volume decreases and completely vanishes for $R = 2fm$. Essentially, the chirally broken phase dissipates leading to a complete crossover region.

V. SUMMARY

In summary, we have discussed the properties of net baryon, net charge and net strangeness fluctuations in nuclear matter within the PNJL model with MRE formalism. The ratio of the fourth to the second order moment and the third to the second order moment of the fluctuations have been considered as observables. All the correlations were obtained by fitting the pressure as a Taylor series expansion around the finite baryon, charge and strangeness chemical potentials. The chemical potentials were obtained from the freeze-out curve which depends on the collision energies in the BES scan in the heavy-ion collision experiments. The results are shown both for the PNJL model with 6 quark interactions and with infinite volume, and two finite volume systems with lateral size $R = 2fm$ and $R = 4fm$. To account for the volume effect, the surface and curvature were included as in the multiple reflection expansion method. These were incorporated in the fermion integrals but not particularly in the Polyakov loop potentials. Model results suggest that as the temperature is increased at zero baryon chemical potential, there is a smooth croosover of the order parameters for both chiral and deconfinement transitions in accordance with lattice QCD results.

An attempt has been also made to compare the model predicted values with experimental results. However, a problem of variable was encountered. While, the model computes the net baryon, net strangeness and net charge; the experimental data is always net proton, net charge and net kaon. This discrepancy has been surmounted with introduction of the subensemble acceptance method to reformulate the experimental data in a grand canonical ensemble. Interestingly, a good quantitative similarity between the reformulated experimental data and the model data has been observed with the incorporation of the subensemble acceptance method.

The phase diagram for the 6 quark PNJL model has also been discussed for both the infinite volume and the finite volume system with $R = 2fm$ and $R = 4fm$ and the critical end point for different system sizes has been discussed. As the system size decreases, the position of the critical points shift towards the lower temperature and chemical potential until it vanishes completely at $R = 2fm$.

The study of various equilibrium thermodynamic measurements of the fluctuations using PNJL model would be helpful in determining the finite temperature finite density behavior of the hadronic sector. Further, a comparison of PNJL results with the experimental value will ensure the understanding of the physics behind the critical region and to locate the critical point in the strongly interacting matter.

ACKNOWLEDGMENTS

P.D would like to thank Women Scientist Scheme A (WOS-A) of Department of Science and Technology (DST) funding with grant no SR/WOS-A/PM-10/2019 (GEN).

[1] STAR Collaboration, J. Adams, and et al., Nuclear Physics A First Three Years of Operation of RHIC, **757**, 102 (2005).
[2] STAR Collaboration, M. M. Aggarwal, and et al., Physical Review C **82**, 024905 (2010).
[3] A. Andronic, P. Braun-Munzinger, and J. Stachel, Nuclear Physics A **772**, 167 (2006).
[4] B. Berdnikov and K. Rajagopal, Physical Review D **61**, 105017 (2000).
[5] M. Stephanov, K. Rajagopal, and E. Shuryak, Physical Review Letters **81**, 4816 (1998).
[6] K. Fukushima, Physics Letters B **591**, 277 (2004).
[7] C. Ratti, M. A. Thaler, and W. Weise, Physical Review D **73**, 014019 (2006).
[8] R. D. Pisarski, Physical Review D **62**, 111501 (2000).
[9] A. Dumitru and R. D. Pisarski, Physics Letters B **525**, 95 (2002).
[10] K. Fukushima, Physical Review D **77**, 114028 (2008).
[11] H. Hansen, W. M. Alberico, A. Beraudo, A. Molinari, M. Nardi, and C. Ratti, Physical Review D **75**, 065004 (2007).
[12] M. Ciminale, R. Gatto, N. D. Ippolito, G. Nardulli, and M. Ruggieri, Physical Review D **77**, 054023 (2008).
[13] S. K. Ghosh, T. K. Mukherjee, M. G. Mustafa, and R. Ray, Physical Review D **73**, 114007 (2006).
[14] S. K. Ghosh, T. K. Mukherjee, M. G. Mustafa, and R. Ray, Physical Review D **77**, 094024 (2008).
[15] P. Deb, A. Bhattacharyya, S. Datta, and S. K. Ghosh, Physical Review C **79**, 055208 (2009).
[16] A. Bhattacharyya, P. Deb, S. K. Ghosh, and R. Ray, Physical Review D **82**, 014021 (2010).
[17] A. Bhattacharyya, P. Deb, A. Lahiri, and R. Ray, Physical Review D **82**, 114028 (2010).
[18] A. Bhattacharyya, P. Deb, A. Lahiri, and R. Ray, Physical Review D **83**, 014011 (2011).

[19] A. Bhattacharyya, P. Deb, S. K. Ghosh, R. Ray, and S. Sur, Physical Review D **87**, 054009 (2013).
[20] A. A. Osipov, B. Hiller, A. H. Blin, and J. da Providência, Annals of Physics **322**, 2021 (2007).
[21] A. A. Osipov, B. Hiller, and J. da Providência, Physics Letters B **634**, 48 (2006).
[22] A. A. Osipov, B. Hiller, V. Bernard, and A. H. Blin, Annals of Physics **321**, 2504 (2006).
[23] B. Hiller, J. Moreira, A. A. Osipov, and A. H. Blin, Physical Review D **81**, 116005 (2010).
[24] K. Kashiwa, H. Kouno, T. Sakaguchi, M. Matsuzaki, and M. Yahiro, Physics Letters B **647**, 446 (2007).
[25] K. Kashiwa, H. Kouno, M. Matsuzaki, and M. Yahiro, Physics Letters B **662**, 26 (2008).
[26] B.-J. Schaefer, J. M. Pawlowski, and J. Wambach, Physical Review D **76**, 074023 (2007).
[27] B.-J. Schaefer and J. Wambach, Physical Review D **75**, 085015 (2007).
[28] B.-J. Schaefer, M. Wagner, and J. Wambach, Physical Review D **81**, 074013 (2010).
[29] J. Wambach, B.-J. Schaefer, and M. Wagner, Acta Phys. Polon. Supp. **3**, 691 (2010).
[30] V. Skokov, B. Friman, E. Nakano, K. Redlich, and B.-J. Schaefer, Physical Review D **82**, 034029 (2010).
[31] P. Chakraborty, M. Mustafa, and M. Thoma, The European Physical Journal C - Particles and Fields **23**, 591 (2002).
[32] P. Chakraborty, M. G. Mustafa, and M. H. Thoma, Physical Review D **68**, 085012 (2003).
[33] N. Haque and M. G. Mustafa, A Modified Hard Thermal Loop Perturbation Theory (2011).
[34] G. Boyd, J. Engels, F. Karsch, E. Laermann, C. Legeland, M. Lütgemeier, and B. Petersson, Nuclear Physics B **469**, 419 (1996).
[35] J. Engels, O. Kaczmarek, F. Karsch, and E. Laermann, Nuclear Physics B **558**, 307 (1999).
[36] Z. Fodor and S. D. Katz, Physics Letters B **534**, 87 (2002).
[37] Z. Fodor, S. D. Katz, and K. K. Szabó, Physics Letters B **568**, 73 (2003).
[38] C. R. Allton, S. Ejiri, S. J. Hands, O. Kaczmarek, F. Karsch, E. Laermann, C. Schmidt, and L. Scorzato, Physical Review D **66**, 074507 (2002).
[39] C. R. Allton, S. Ejiri, S. J. Hands, O. Kaczmarek, F. Karsch, E. Laermann, and C. Schmidt, Physical Review D **68**, 014507 (2003).
[40] C. R. Allton, M. Döring, S. Ejiri, S. J. Hands, O. Kaczmarek, F. Karsch, E. Laermann, and K. Redlich, Physical Review D **71**, 054508 (2005).
[41] P. de Forcrand and O. Philipsen, Nuclear Physics B **642**, 290 (2002).
[42] Y. Aoki, G. Endrődi, Z. Fodor, S. D. Katz, and K. K. Szabó, Nature **443**, 675 (2006).
[43] Y. Aoki, Z. Fodor, S. D. Katz, and K. K. Szabó, Physics Letters B **643**, 46 (2006).
[44] E. Megias, E. R. Arriola, and L. L. Salcedo, Romanian Reports in Physics **58**, 81 (2006).
[45] E. Megías, E. Ruiz Arriola, and L. L. Salcedo, in *Proceedings of 29th Johns Hopkins Workshop on current problems in particle theory: strong matter in the heavens PoS (JHW 2005)*, Vol. 22 (SISSA Medialab, 2006) p. 025.
[46] E. Megías, E. R. Arriola, and L. L. Salcedo, Nuclear Physics B - Proceedings Supplements Proceedings of the QCD 08, 14th High-Energy Physics International Conference On Quantum ChromoDynamics, **186**, 256 (2009).
[47] E. Megías, E. R. Arriola, and L. L. Salcedo, Physical Review D **81**, 096009 (2010).
[48] S. Ejiri, F. Karsch, and K. Redlich, Physics Letters B **633**, 275 (2006).
[49] S. Rößner, C. Ratti, and W. Weise, Physical Review D **75**, 034007 (2007).
[50] C. Sasaki, B. Friman, and K. Redlich, Physical Review D **75**, 074013 (2007).

[51] S. Mukherjee, M. G. Mustafa, and R. Ray, Physical Review D **75**, 094015 (2007).
[52] A. Bhattacharyya, R. Ray, and S. Sur, Physical Review D **91**, 051501 (2015).
[53] Y. Nambu and G. Jona-Lasinio, Physical Review **122**, 345 (1961).
[54] H.-T. Elze and W. Greiner, Physics Letters B **179**, 385 (1986).
[55] M. Lüscher, Communications in Mathematical Physics **104**, 177 (1986).
[56] J. Gasser and H. Leutwyler, Physics Letters B **188**, 477 (1987).
[57] O. Kiriyama and A. Hosaka, Physical Review D **67**, 085010 (2003).
[58] G.-y. Shao, L. Chang, Y.-x. Liu, and X.-l. Wang, Physical Review D **73**, 076003 (2006).
[59] J. Braun, B. Klein, and P. Piasecki, The European Physical Journal C **71**, 1576 (2011).
[60] J. Braun, B. Klein, and B.-J. Schaefer, Physics Letters B **713**, 216 (2012).
[61] A. Gopie and M. C. Ogilvie, Physical Review D **59**, 034009 (1999).
[62] A. Bazavov and B. A. Berg, Physical Review D **76**, 014502 (2007).
[63] R. Balian and C. Bloch, Annals of Physics **60**, 401 (1970).
[64] J. Madsen, Physical Review D **50**, 3328 (1994).
[65] A. G. Grunfeld and G. Lugones, The European Physical Journal C **78**, 640 (2018).
[66] V. Vovchenko, O. Savchuk, R. V. Poberezhnyuk, M. I. Gorenstein, and V. Koch, Physics Letters B **811**, 135868 (2020).
[67] J. Cleymans, H. Oeschler, K. Redlich, and S. Wheaton, Physical Review C **73**, 034905 (2006).
[68] F. Karsch and K. Redlich, Physics Letters B **695**, 136 (2011).
[69] S. Borsányi, Z. Fodor, C. Hoelbling, S. D. Katz, S. Krieg, and K. K. Szabó, Physics Letters B **730**, 99 (2014).
[70] Gnuplot :an interactive plotting program, http://gnuplot.sourceforge.net/.
[71] STAR Collaboration, L. Adamczyk, and et al., Physical Review Letters **113**, 092301 (2014).
[72] STAR Collaboration, L. Adamczyk, and et al., Physical Review Letters **112**, 032302 (2014).
[73] L. Adamczyk and et al., Physics Letters B **785**, 551 (2018).
[74] C. Collaboration, Two-particle Bose-Einstein correlations and their l'evy parameters in PbPb collisions at $\sqrt{S_{NN}} = 5.02$ TeV (2023).